Self-Assembly of Artificial Nucleobase 1H-Benzimidazole-4,7-dione at the Liquid/Solid Interface

ARTICLE *in* THE JOURNAL OF PHYSICAL CHEMISTRY B · JULY 2009

Impact Factor: 3.3 · DOI: 10.1021/jp9029419 · Source: PubMed

Self-Assembly of Artificial Nucleobase 1*H*-Benzimidazole-4,7-dione at the Liquid/Solid Interface

Wael Mamdouh,*[,†,‡] Ross E. A. Kelly,[§,||] Mingdong Dong,[†,‡,⊥] Mikkel F. Jacobsen,[†,#] Elena E. Ferapontova,[†,#] Lev N. Kantorovich,[||] Kurt V. Gothelf,[†,#] and Flemming Besenbacher*[,†,‡]

Centre for DNA Nanotechnology (CDNA), The Interdisciplinary Nanoscience Center (iNANO), and Departments of Physics and Astronomy and of Chemistry, Aarhus University, DK-8000 Aarhus C, Denmark, Department of Physics and Astronomy, University College London (UCL), Gower Street, London WC1E 6BT, United Kingdom, and Department of Physics, School of Physical Sciences and Engineering, King's College London, Strand, London WC2R 2LS, United Kingdom

Received: March 31, 2009; Revised Manuscript Received: April 30, 2009

Self-assembly at the liquid/solid interface of an electrochemically active DNA nucleobase analogue, 1*H*-benzoimidazole-4,7-dione (Q), has been studied by means of scanning tunneling microscopy (STM). High-resolution STM images revealed the formation of well-ordered two-dimensional (2D) supramolecular nanostructures when the Q molecules are adsorbed onto the graphite surface from a 1-octanol solution. Detailed analysis shows that the observed 2D nanostructures are mainly dominated by hydrogen-bonded Q molecules. Since Q can be considered as a molecule mimicking the nucleobase guanine (G), which is known to form Watson−Crick base pairs with its complementary nucleobase cytosine (C), we have examined the binding ability of Q with C realized by available hydrogen-bonding sites on both Q and C molecules. Upon deposition of a mixture of Q and C molecules onto a graphite surface, one might expect that hydrogen-bonded QC dimers were observed in a new 2D self-assembled structure governed by *inter*- and *intra*molecular hydrogen-bonding interactions between Q and C molecules. However, our STM experiments showed that no well-ordered structures are formed and instead phase separation occurs where large-scale homodomains are formed consisting of the individual QQ and CC dimers. To gain further insight into the possible molecular arrangements of the Q and C nucleobases in the mixture phase, the high-resolution STM images are compared with the results from ab initio density functional theory (DFT) calculations.

1. Introduction

Quinones are an important class of compounds with interesting biochemical and electrochemical properties, which are involved as electron and proton carriers in a variety of biochemical processes, where hydrogen bond formation plays a key role in stabilization of the reduced quinone species.[1,2] Quinones show well-defined pH-dependent quinone/hydroquinone redox potentials.[3] In DNA research, various redox-active benzoquinone derivatives, e.g., anthraquinone, have been incorporated into oligonucleotides or used as external intercalators for the detection of hybridization events,[4−8] strand cleavage,[9,10] and single-base mismatches (SNPs)[11,12] and in studies of electron transfer in DNA.[13] These approaches have mainly focused on π-stacking interactions between the quinone moiety and nucleobases. However, both from fundamental and biochemical points of view and within the area of DNA technology, planar structures of DNA nucleobases and quinones based on hydrogen bonding may be of great interest in the development of novel DNA-based nanostructures.

Hydrogen bonding between nucleobases, in addition to $\pi-\pi$ stacking, is one of the main interactions that control the molecular conformation of double-stranded oligonucleotides and hence its biochemical functions. In nature, the exquisite bonding specificity between complementary nucleobases in DNA proceeds via intermolecular hydrogen bonding.[14] The selective hydrogen bonding between nucleobase molecules also underlies the transfer of genetic information in biological processes.[15] Hydrogen bonds can be used as a driving force of a more efficient design of 2D self-assembled supramolecular architectures in organic chemistry and may play an important role in novel biosensors based on surface functionalization with ssDNA oligomers.[16,17] DNA/RNA strands are also suitable for the design and formation of self-assembled (artificial) nanostructures, since it is possible to use their base sequences to encode instructions for assembly in a predetermined fashion at the nanometer scale.[18−21]

Scanning tunneling microscopy (STM) has proven to be a remarkable technique to reveal the atomic scale realm of matter.[21−27] More specifically, submolecular resolution has been achieved of supramolecular assemblies of individual and complementary nucleobase molecules on several substrates and under a wide variety of experimental conditions.[28−51]

The nucleobase molecule guanine (G) is well-known for its ability to form various self-assembled structures, e.g., quadruplexes,[52] under well-controlled ultra-high-vacuum (UHV) conditions, and 2D G monolayers have recently been observed on the Au(111)[33] and graphite[28,50] surfaces. In comparison, the DNA

* To whom correspondence should be addressed. E-mail: wael@inano.dk and fbe@inano.dk.
† CDNA, iNANO, Aarhus University.
‡ Department of Physics and Astronomy, Aarhus University.
§ UCL.
|| King's College London.
⊥ Present address: Rowland Institute at Harvard, Harvard University, Cambridge, MA 02142.
Department of Chemistry, Aarhus University.

10.1021/jp9029419 CCC: $40.75
Published on Web 06/01/2009

nucleobase cytosine (C) has been observed under UHV conditions on the Au(111) surface to assemble into highly mobile disordered structures which demonstrate properties of a 2D glass when quickly cooled to low temperature.[39,40] The coadsorption of these complementary nucleobases G and C on a Au(111) surface,[49] and separately on a graphite surface in a 1-octanol solvent,[47] results in the formation of characteristic Watson−Crick (WC) base pairs between the C and G molecules. Similarly, the coadsorptions of G with the RNA nucleobase molecule uracil (U)[50] and also of adenine (A) with thymine (T) were observed to lead to the formation of 2D periodic hydrogen-bonded patterns.[48]

Here we report on STM studies of the self-assembly of an electrochemically active nucleobase analogue, 1*H*-benzoimidazole-4,7-dione (Q),[53] at the liquid/solid interface. Q is a quinone derivative with a steric resemblance to G, and this compound may be an interesting candidate for the design of novel DNA nanostructures. In addition, voltammetry studies have been used to determine the Q surface coverage in a complementary way.

2. Experimental and Computational Section

The STM experiments were performed at the liquid (1-octanol)/solid (highly oriented pyrolytic graphite (HOPG)) interface at room temperature under ambient conditions using a MultiMode SPM system with a Nanoscope IIIa controller (Veeco Instruments Inc., Santa Barbara, CA) along with an external pulse/function generator (model HP 8111 A). STM tips were mechanically cut from a 0.25 mm Pt/Ir (80:20) wire and tested on freshly cleaved HOPG surfaces (grades ZYA and ZYB, Advanced Ceramics Inc., Cleveland, OH, and NT-MDT, respectively). Prior to the STM imaging, Q, synthesized following a previously described procedure,[53] and C (Sigma Aldrich, 99% purity) were separately dissolved in 1-octanol (Sigma Aldrich, 99.5% purity) at concentrations of 1.2 mg/g for Q (6.7 mM) and 3 mg/3g for C (7.4 mM), and a drop of each solution was applied onto a freshly cleaved surface of HOPG, resulting in the formation of either Q or C structures. To prepare the coexisting Q + C mixture, we mixed the solution of Q dissolved in 1-octanol with the solution of C dissolved in 1-octanol (with a 1:1 mixing molar ratio), and one drop of the Q + C mixture was deposited onto a freshly cleaved HOPG surface. Subsequently, the STM tip was immersed in each of the three solutions, and STM images were recorded at the 1-octanol/graphite interface.

Several STM tips and HOPG samples were used to ensure that reproducible results are obtained and to avoid any artifacts related to the STM imaging. The STM images were all recorded in constant current mode. For a proper unit cell calibration of the STM images of the Q and C molecular nanostructures, the recording of the molecular STM images was subsequently followed by imaging the underlying virgin graphite substrate under the same experimental conditions, by lowering the bias voltage. The STM images were analyzed using the Scanning Probe Image Processor (SPIP) software program (Image Metrology ApS, Lyngby, Denmark),[54] and the STM images were corrected for any drift using the recorded graphite calibration images, which allowed us to determine the unit cells accurately. Furthermore, the correlation averaging method[55] was used for a more detailed image analysis and for displaying high-resolution STM images. We always investigated very thoroughly that this method did not affect the unit cell parameters. The imaging parameters (tunneling current, I_{tunn}, and sample bias voltage, V_{bias}) are stated in the figure captions.

Voltammetry measurements were performed with a three-electrode potentiostat, AUTOLAB PGSTAT 302 (Eco Chemie B.V., Utrecht, The Netherlands), connected to a 2 mL Teflon electrochemical cell, in which the HOPG working electrode (0.79 cm^2 area) represented the bottom of the cell. A Ag/$AgCl_{0.1\ M\ (TBA)Cl}$ octanol electrode was used as the reference, and a Pt spiral wire was used as the auxiliary electrode. Adsorption conditions were similar to those used in STM experiments, except that the 1-octanol solution contained 0.1 M (TBA)Cl as the electrolyte.

SCHEME 1: Chemical Structures of (A) 1*H*-Benzoimidazole-4,7-dione (Q) and (B) Cytosine (C)[a]

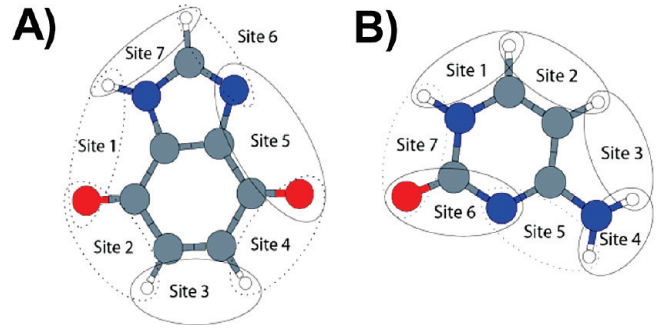

[a] The hydrogen-bonding sites are marked by ovals and numbered. The colors used are blue for nitrogen, red for oxygen, gray for carbon, and white for hydrogen atoms.

To gain further atomistic insight into the observed STM images, theoretical calculations of the Q, C, and Q + C pairs, as well as larger structures such as one-dimensional (1D) chains and 2D monolayers, were performed using the ab initio DFT SIESTA method.[56,57] In short, SIESTA uses a localized numerical atomic orbital basis set, the method of pseudopotentials, and periodic boundary conditions. The DZP (double-ζ plus polarization orbitals) basis set was used with an appropriate energy cutoff of 10 meV. The Perdew, Becke, and Ernzerhof (PBE) density functional was used for the exchange-correlation functional. Atomic relaxation was considered complete when the forces on each atom were not larger than 0.05 eV/Å. Note that no constraints were applied during the relaxations and that all molecular structures, which were considered without the surface due to the expected weak surface corrugation potential, relaxed into relatively planar configurations. Due to the large cell sizes, only one (γ) k-point was required for these calculations. The basis set superposition error (BSSE) corrections were included because they are known to be essential to obtain reliable binding energies in localized basis set calculations. Note that this ab initio technique has been extensively tested for DNA and RNA homopairs[58−60] and a large selection of heteropairs[61] involving DNA and RNA bases by comparison with benchmark quantum chemistry (QC) calculations,[62] where a very good agreement was found.

To gain further insight into which supramolecular nanostructures that may form from pure Q, pure C, or the QC mixture, we have exploited a systematic methodology. Our method is based on identifying for each molecule the available binding sites, which can form double hydrogen bonds between two molecules. Next, we explore how the molecules can adjoin to form larger network structures. Suitable structures are then relaxed using the ab initio DFT SIESTA methods.

In Scheme 1 the chemical structures of Q and C are depicted together with all other possible binding sites. Similar to the other nucleobase molecules, dimers are the simplest structures that can form, and detailed analysis of all possible dimers resulting from the Q and C molecules is the initial stage in our analysis for identifying all possible 1D and 2D structures.[58,63]

In the following, the notation X_nY_m is adopted to indicate dimers formed by the two molecules, where X and Y correspond to either Q or C, and the indices n and m correspond to the particular binding sites on X and Y as depicted in Scheme 1. We shall also indicate in parentheses the relative position the dimers occupy when ordered in terms of their stability, with the most stable being listed first.

3. Results and Discussion

STM Results. In the initial control experiments, high-resolution STM images of 2D supramolecular networks of individual Q molecules at the 1-octanol/graphite interface were obtained, as depicted in Figure 1.

Large-scale 2D self-assembled Q monolayers are formed (Figure 1A) with a periodic structure containing two Q molecules per unit cell and with lattice vectors indicated in Table 1. In Figure 1B a high-resolution image of a selected part of the image of Figure 1A is shown. It is seen to contain a collection of periodically distributed bright and dim spots, and each spot is tentatively associated with one Q molecule.

In Figure 1, we have also depicted the corresponding relaxed theoretical model originating from our ab initio calculations. The QQ dimers, which form the periodic structural motif, are indicated with yellow ovals in the STM image in Figure 1B and also on the molecular model in Figure 1C. The proposed molecular DFT model in Figure 1C is found to be in very good agreement with the 2D self-assembled supramolecular Q networks depicted in the STM images in Figure 1A,B.

The surface coverage of Q was determined electrochemically by integrating the voltammetric peak of oxidation of the Q imidazole ring and was found to be $(1.7 \pm 0.5) \times 10^{-10}$ mol cm^{-2}, which is consistent with a Q monolayer surface coverage determined from the STM data as those in Figure 1A,B (1.5 molecules per nm^2 or 2.5×10^{-10} mol cm^{-2}) (see the Supporting Information, Figure SI.1).

Figure 2 indicates the two most stable Q pairs, $Q_1Q_1(1)$ and $Q_1Q_6(2)$ with stabilization energies of -0.69 and -0.60 eV, respectively. In our calculations we also found other less stable dimer configurations with energies ranging between -0.13 and -0.46 eV; these are not depicted here. Also shown in Figure 2 are three QQ 1D chain structures that may form from the two most stable dimers, Q_1Q_1 and Q_1Q_6. These 1D chains contain two, two, and four molecules in the unit cells, respectively, and the calculated stabilization energies of the 1D chains (per unit cell) are -0.90, -0.80, and -1.66 eV (or -0.83 eV per two molecules), respectively.

By attaching the most favorable chains parallel to each other, 2D monolayer structures can be constructed. In Table 2 the geometric and energetic characteristics are depicted for the theoretically obtained self-assembled Q monolayer 2D structures.

It should be mentioned that theoretically two high-energy stable Q monolayer structures are possible with similar (per two molecules) binding energies, both based on the Q_1Q_6 dimer, one with two and another with four molecules in the unit cell. In the STM images, the latter monolayer structure may easily be viewed as consisting of two molecules in the cell (see Table 2); i.e., this monolayer structure may mimic a structure with two molecules in the unit cell. Hence, two possibilities appear to exist for the Q monolayer structure. In fact, when the two Q_1Q_6 monolayer possibilities are compared (see Figure 3), they indeed appear extremely similar.

Interestingly, however, the structure with two molecules per unit cell produces homochiral domains, i.e., all molecules have the same chirality, whereas the other monolayer structure with four molecules in the unit cell is heterochiral, i.e., it consists of an equal distribution of molecules of both chiralities. By flipping Q molecules of one chirality or by simultaneous proton transfer between connected molecules, the two structures turn each other as illustrated in Figure 3. In fact, a very similar situation exists in the case of A.[38] It is expected that the barrier for the proton

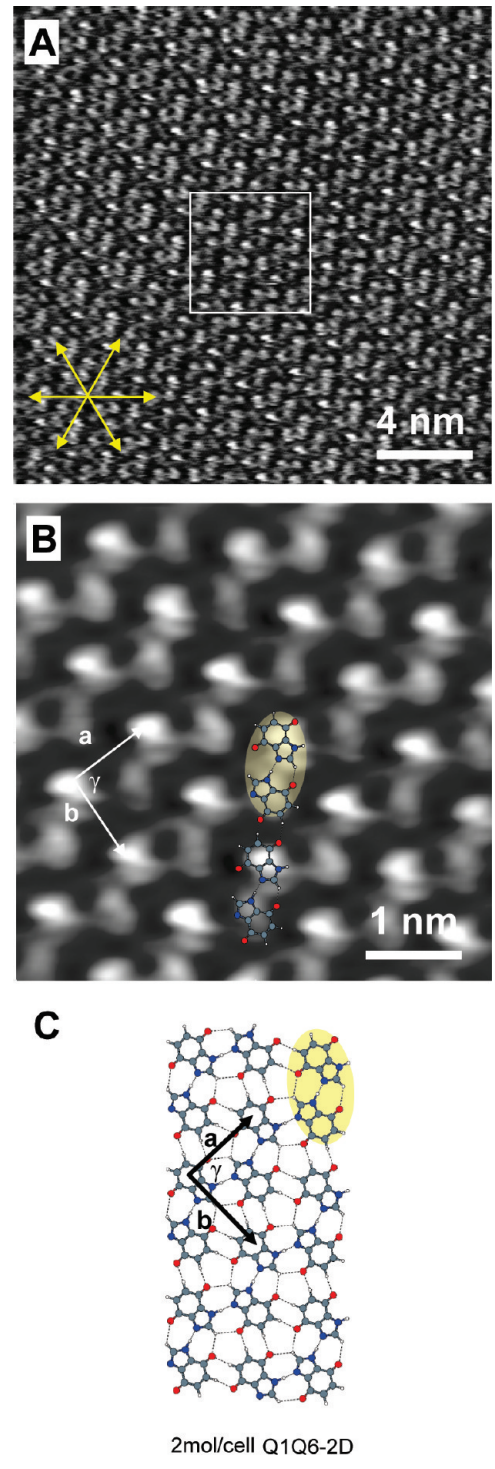

Figure 1. High-resolution STM images of Q self-assemblies at the 1-octanol/graphite interface. The tunneling parameters are $I_{tunn} = 1.029$ nA and $V_{bias} = 402$ mV. (B) Magnified inset of the white square in (A). (C) QQ 2D monolayer structure proposed to explain the observed STM image in (B) and relaxed using our ab initio DFT method. QQ dimers are illustrated with yellow ovals. The unit cells are also indicated by vectors **a** and **b**, as well as by the angle γ between them. 1D chains are superimposed on the STM image in (B) for display purposes. The graphite axes are indicated in yellow in (A).

TABLE 1: Lattice Parameters[a]

	experimental			calculated		
	a (nm)	**b** (nm)	γ (deg)	**a** (nm)	**b** (nm)	γ (deg)
quinone	1.00 ± 0.10	0.90 ± 0.10	89 ± 2.0	0.97	1.03	90.1
cytosine	0.80 ± 0.20	0.70 ± 0.20	109 ± 2.0	0.93	1.00	103.0
				1.40	1.01	90.0
Q_1C_5	X	X	X	1.02	0.95	88.5
Q_1C_7	X	X	X	1.22	0.92	64.1

[a] "X" means that no high-resolution experimental STM images have been observed for the Q + C mixture.

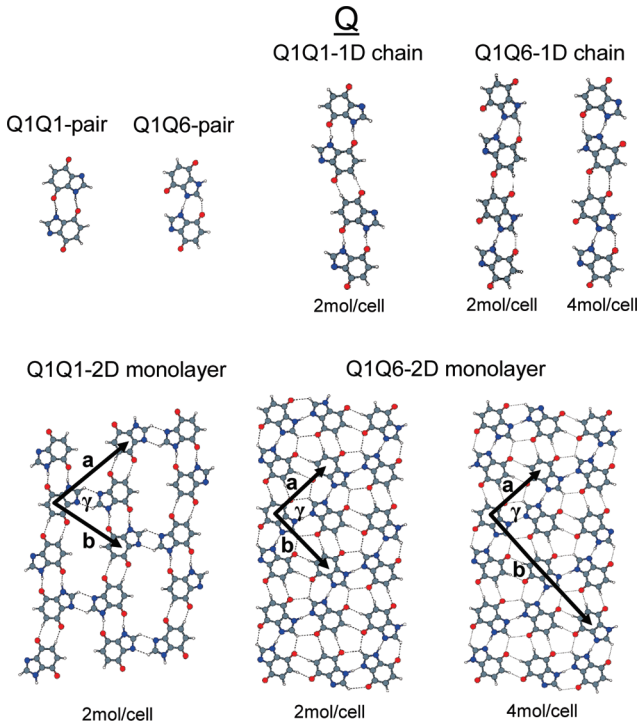

Figure 2. DFT-relaxed QQ pairs, 1D chains, and 2D monolayers.

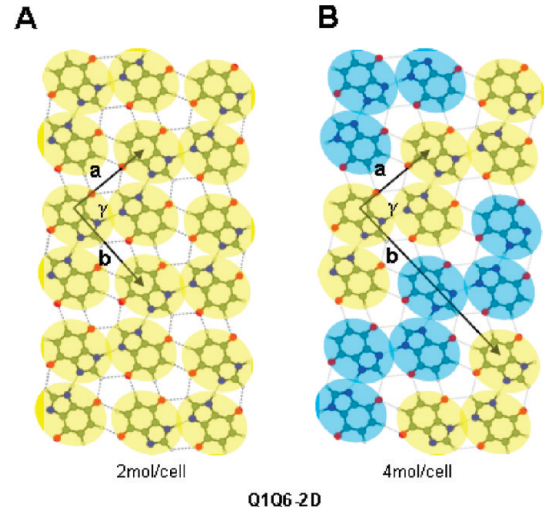

Figure 3. Structural models of a homochiral Q_1Q_6 2D monolayer with two molelcules per cell (A) and a heterochiral Q_1Q_6 2D monolayer with four molecules per cell (B), relaxed with our ab initio DFT method. The colors are used to indicate the chirality of the Q molecules.

transfer is lower than for the molecules' flipping although the solvent may assist in the latter process so that this mechanism may also be accessible.

We have also recorded STM images of the pure C monolayer structure that reveal chains of bright spots which are attributed to one-dimensional (1D) filaments of C dimers aligned parallel to each other, with two molecules in the unit cell (see Figure 4) and with lattice vectors as indicated in Table 1. We have also constructed and relaxed the corresponding theoretical model based on our ab initio calculations as shown in Figure 5. The CC dimers, which form the periodic structural motif, are indicated with yellow ovals in the STM image in Figure 4A and also on the molecular models in Figure 4B. The proposed molecular DFT models in Figure 4B are found to be in very good agreement with the C networks depicted in the STM image in Figure 4A.

In Figure 5 the three most stable C pairs, $C_7C_7(1)$, $C_7C_5(2)$, and $C_5C_5(3)$ (with stabilization energies of −0.99, −0.96, and −0.87 eV, respectively,[58] are depicted. They may join to form the two most dominant chains, C_7C_5 1D and $C_7C_7C_5C_5$ 1D, with stabilities of −1.89 and −1.82 eV per unit cell, respectively. Both 1D chains have two molecules in the unit cell. Also for the CC 2D self-assembled monolayer, two plausible theoretical configurations exist (as proposed in Figure 4 and 5) based on the two most stable 1D chains, which join parallel to each other to form 2D monolayers. It is assumed that the chains are bound together via van der Waals (vdW) interactions as there are no matching binding sites available to form hydrogen bonds between parallel chains. It is interesting to note that, under the extreme, well-controlled UHV conditions no such CC 2D monolayer structures have been observed on the Au(111)

TABLE 2: Theoretically Calculated 2D Monolayer Possibilities

monolayers based on pair	no. of molecules in unit cell	**a** (nm)	**b** (nm)	γ (deg)	E_{BSSE} (eV)	E_{int}(eV)	E_{def} (eV)	E_{stab} (eV)
Q_1Q_6	2	0.97	1.03	90.1	0.41	−1.95	0.30	−1.66
Q_1Q_6[a]	4	0.97	1.05	89.8	0.41	−1.90	0.26	−1.64
Q_1Q_1	2	1.27	1.04	73.9	0.34	−1.26	0.11	−1.14
C_7C_5[b]	2	0.93	0.95	100.3	0.39	−2.46	0.57	−1.89
C_7C_7[b]	2	1.01	0.95	103.0	0.34	−2.40	0.59	−1.82
Q_1C_5	2	1.02	0.95	88.5	0.39	−1.85	0.25	−1.60
Q_1C_7	2	1.22	0.92	64.1	0.36	−1.82	0.27	−1.56

[a] All energies and the lattice vector **a** for this structure with four molecules in the cell are divided by 2 for ease of comparison with those of other lattices containing two molecules in the cell. [b] The lattice vector **a** and the angle γ in these cases can only be considered as estimates since DFT does not account for the van der Waals interaction between filaments running parallel to each other in the structures.

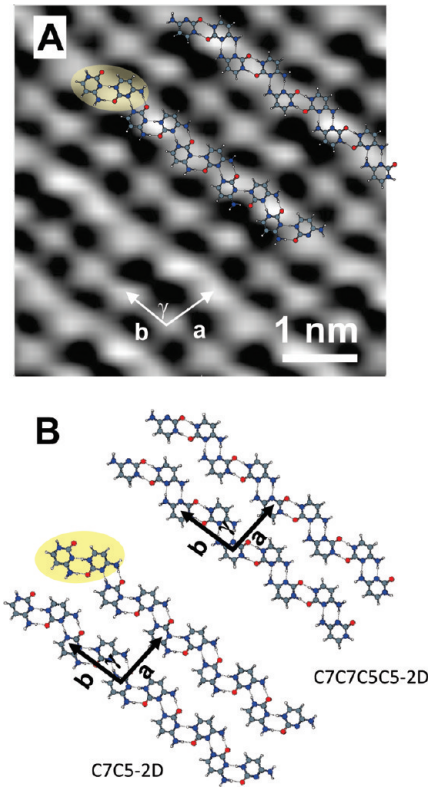

Figure 4. (A) High-resolution STM image of C self-assemblies at the 1-octanol/graphite interface. The tunneling parameters are $I_{tunn} = 0.605$ nA and $V_{bias} = 700$ mV. (B) Ab initio DFT calculation models of CC 2D monolayer structures proposed to explain the observed STM image in (A). CC dimers are illustrated with yellow ovals. The unit cells are also indicated by basic vectors **a** and **b**, as well as by the angle γ between them. 1D chains are superimposed on the STM image for display purposes.

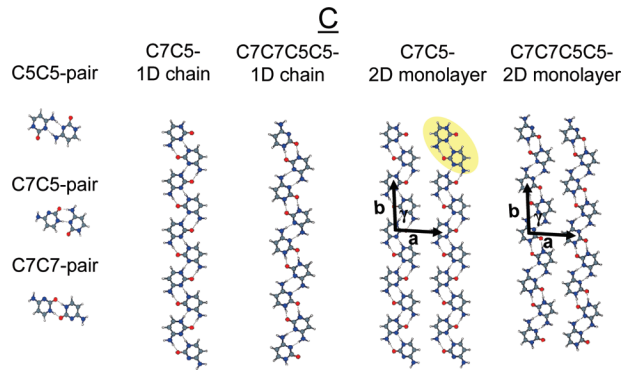

Figure 5. DFT-relaxed CC pairs, 1D chains, and 2D monolayers.

surface, although it was argued[39,40] that this structure should correspond to the most stable C structure on gold. We therefore tentatively suggest that the solution used in the present experiments helps in catalyzing the formation of the C ground-state structure. Note that since the theoretical DFT calculations do not incorporate the vdW interactions, the binding energies for the two C monolayers given in Table 2 as −1.89 and −1.82 eV are underestimated and correspond to those of the noninteracting 1D chains.

More interestingly, we have also examined (theoretically by our ab initio DFT calculations and experimentally by STM at the 1-octanol/graphite interface) the binding possibility between Q and C, due to the availability of matching hydrogen-bonding sites on both Q and C molecules. Eventually, one might expect that upon mixing both Q and C molecules, hydrogen-bonded QC dimers will form and most probably act as the building blocks for a completely new 2D self-assembled structure upon adsorption on the graphite surface and that these 2D structures will be governed by inter- and intramolecular hydrogen bonding between the Q and C molecules.

We carried out ab initio DFT calculations on the QC mixture, and the proposed models are shown in Figure 6.

In Figure 6, the most stable QC pairs, $Q_1C_7(1)$ and $Q_1C_5(2)$, are shown with energies of −0.91 and −0.90 eV, respectively. Again, these may form their respective chains Q_1C_7 1D and Q_1C_5 1D with two molecules in the cell each and with energies of −1.28 and −1.39 eV per unit cell, respectively. In addition, we include in Figure 6 the WC QC pair Q_4C_5 (−0.41 eV), which mimics the most stable WC G + C pair.

For the calculated Q + C monolayer, two structures with different periodicities (see Tables 1 and 2) shown in Figure 6 appear to be the two most stable structures. These two structures have very similar binding energies (Table 2). However, very surprisingly, when we have prepared the mixture (with equimolar ratios) of the individual Q and C molecules in 1-octanol solution at room temperature (RT), and a drop of the QC mixture was deposited onto the bare graphite surface, no well-ordered structures were formed from the QC mixture, and instead, phase separation occurs where large-scale homodomains were formed by the individual QQ and CC dimers, similar to the domains observed in the control experiments in Figure 1 for Q and in Figure 4 for C.

Additionally, in the electrochemical experiments, it was also found that when Q was coadsorbed with C, only $(1.1 \pm 0.3) \times 10^{-10}$ mol cm^{-2} Q underwent electrochemical oxidation, which is consistent with a lower surface concentration of Q compared to the pure Q monolayer. However, these data do not clearly support or explain the situation with the formation of QQ and CC homodomains during the codeposition process.

In addition to the separated Q and C homodomains, some additional fuzzy structures also appear in the STM images on top of some long-range ordered homodomains, corresponding to some mobile assemblies, which seem to "diffuse" on top of the existing monolayers (see Figure SI.2, Supporting Information). These mobile islands are distinctly different in appearance from the QQ and CC homodomains, which suggest that they may be related to transitional or weakly bound disordered heterodomains formed by the QC mixture that is weakly interacting (presumably by vdW forces) with the layer underneath. This may explain their mobility during the STM scanning, and this may be one of the reasons why no ordered QC domains were observed in the STM experiments.

Hence, we have not observed any stable mixed Q + C self-assembled monolayer structures on the surface in our STM experiments. The reason for this is not completely clear. It follows from our DFT calculations that the mixed QC dimers are energetically more favorable than the QQ dimers (see the energies listed in Table 2), so one may argue that it is surprising that the energetically more favorable QC dimers apparently do not form on the surface when the QC mixture is deposited. One tentative explanation is that, prior to the deposition of the QC mixture on the surface, substantial interaction between the Q and between the C single molecules in *their respective solutions* might have occurred, leading to the possibility that QQ and CC dimers may have formed larger "pure" Q and C clusters of molecules such as trimers, tetramers, etc. with very small numbers of single molecules left; i.e., the segregation already happened in the mixed solution prior to its deposition. Note that C molecules in solution (prior to deposition) may only form

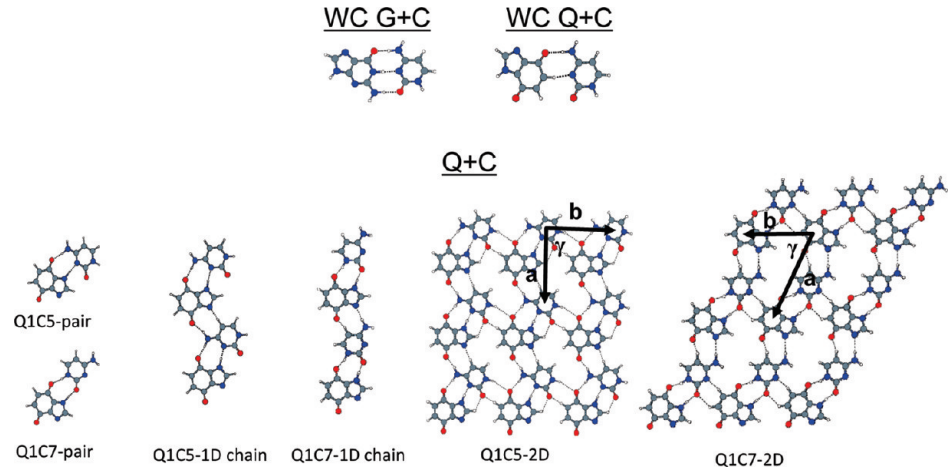

Figure 6. Structural models of QC pairs that are used to construct QC 1D chains and 2D monolayers, respectively, all relaxed using our ab initio DFT method. The top panel shows the most stable WC G + C pair and its corresponding mimic, the WC Q + C pair.

disordered planar clusters[39,40] with less than three molecules hydrogen bonded to any C molecule; 1D chains may also bind together by weak vdW forces, but these ordered 2D structures can easily be broken by thermal motion in the solution. At the same time, the Q molecules may form ordered 2D structures (Figure 2) where each Q molecule binds to four neighboring molecules. However, taking into account the calculated monolayer energies, we find that disordered C clusters are still on average more favorable (per molecule) than possible Q clusters: −0.95 eV for C_7C_5 2D and −0.91 eV for $C_7C_7C_5C_5$ 2D (even assuming every C molecule is bound to only two other Q molecules, e.g., in a 1D chain) against −0.83 and −0.82 eV for the Q_1Q_6 2D monolayers containing two and four Q molecules per unit cell, respectively. Therefore, one may tentatively anticipate on the basis of the DFT calculations that, in the mixture solution, prior to deposition, large C planar clusters exist, while Q planar clusters are smaller and less stable. Consequently, when this mixture is deposited on the surface, formation of large Q + C monolayers is kinetically trapped by already preexisting C and (in a lesser extent) Q clusters, and this is why we do not observe QC self-assembled monolayers.

Another possible explanation might be that the segregation of Q and C molecules on the surface occurs catalytically by the interaction with the graphite surface, which we cannot account for or explore in our gas-phase calculations of the monolayers described above. This explanation may be supported by the images of fuzzy domains observed in Figure SI.2A,D, Supporting Information, which tend to indicate that these domains consist of small clusters of Q and C molecules. This explanation would also account for the effects observed in Figure SI.2. It is similar to the previous observation in our UHV studies that non-cDNA bases (A + C) segregate on the Au(111) surface, whereas G + C structures survive after annealing, forming Watson−Crick base pairs.[49] In spite of the fact that Q is geometrically similar to G, the binding energies for the G + C WC pair (−1.12 eV)[61] and the corresponding Q + C pair (−0.41 eV) differ quite a lot. This is due to the fact that the G + C pair forms three strong H-bonds in the WC configuration, whereas the Q + C pair is only able to form one strong and one much weaker H-bond as depicted in Figure 6. Thus, the behavior of Q and C is different from that of G and C, and Q is probably not very appropriate as a G-mimicking structure. Even the more stable possibilities Q_1C_7 (−0.91) and Q_1C_5 (−0.90) do not have stabilities comparable to that of the GC WC pair, and the same applies even to the most stable C_7C_7 (−0.99) and C_7C_5 (−0.96) pairs.[58]

4. Conclusions

We have studied the formation of 2D self-assembled supramolecular nanostructures formed by Q and C molecules separately, as well as the adsorption of a QC mixture at the 1-octanol/graphite interface by STM. Surprisingly, upon mixing of Q and C molecules, no well-ordered self-assembled structures were formed, and instead, phase separation into Q and C domains occurred. On top of the well-ordered homo-Q and -C supramolecular domains, highly mobile domains appear with fuzzy STM contrast. These very mobile domains may be related to the formation of QC mixtures. The electrochemically determined Q monolayer surface coverage was in a good agreement with the coverage determined by STM.

These surface studies demonstrate that by using a guanine-mimic compound such as Q, which has lower hydrogen-bonding multiplicity than G, the self-assembled 2D nanostructures will be altered accordingly, leading to phase separation. On the other hand, the use of Q as G surrogates in dsDNA should differ significantly in the sense that the position of Q is more fixed, and thus, its interactions with C may be stronger. Further electrochemical studies of the interaction between the artificial redox-active nucleobase Q and the nucleobases in dsDNA are in progress and will be reported elsewhere.

Acknowledgment. We acknowledge financial support from the Danish National Research Foundation and the Danish Ministry for Science, Technology, and Innovation through the iNANO Center from the Danish Research Councils. R.E.A.K. is also grateful to the EPSRC for financial support (Grant GR/P01427/01).

Supporting Information Available: Figures SI.1 showing the voltammogram for electrochemical oxidation of Q adsorbed on the HOPG electrode, Figure SI.2 showing the STM images obtained after deposition of the Q + C mixture at the 1-octanol/graphite interface, and text with a further description of the information contained in Figure SI.2. This material is available free of charge via the Internet at http://pubs.acs.org.

References and Notes

(1) *The Chemistry of the Quinoid Compounds*; Patai, S., Ed.; Wiley: New York, 1988.

(2) Cramer, W. A.; Knaff, D. B. In *Energy Transduction in Biological Membranes*; Cantor, C. R., Ed.; Springer-Verlag: New York, 1990.

(3) Laviron, E. *J. Electroanal. Chem.* **1984**, *164*, 213–227.

(4) Piro, B.; Reisberg, S.; Noel, V.; Pham, M. C. *Biosens. Bioelectron.* **2007**, *22*, 3126–3131.
(5) Yamana, K.; Kumamoto, S.; Hasegawa, T.; Nakano, H.; Sugie, Y. *Chem. Lett.* **2002**, 506–507.
(6) Tanabe, K.; Iida, H.; Haruna, K.-I.; Kamei, T.; Okamoto, A.; Nishimoto, S.-I. *J. Am. Chem. Soc.* **2006**, *128*, 692–693.
(7) Wong, E. L. S.; Gooding, J. *J. Anal. Chem.* **2003**, *75*, 3845–3852.
(8) Jakobsen, M. F.; Ferapontova, E. E.; Gothelf, K. V. *Org. Biomol. Chem.* **2009**, *7*, 905–908.
(9) Tanabe, K.; Yamada, H.; Nishimoto, S.-I. *J. Am. Chem. Soc.* **2007**, *129*, 8034–8040.
(10) Bergeron, F.; Klarskov, K.; Hunting, D. J.; Wagner, J. R. *Chem. Res. Toxicol.* **2007**, *20*, 745–756.
(11) Okamoto, A.; Kamei, T.; Saito, I. *J. Am. Chem. Soc.* **2005**, *128*, 658–662.
(12) Orino, N.; Kumamoto, S.; Nakamura, M.; Yamana, K. *Nucleic Acids Symp. Ser.* **2005**, *49*, 139–140.
(13) Wagenknecht, H.-A. *Nat. Prod. Rep.* **2006**, *23*, 973–1006.
(14) Saenger, W. *Principles of Nucleic Acid Structure*; Springer: Berlin, 1984.
(15) Watson, J. D.; Crick, F. C. H. *Nature* **1953**, *171*, 737–738.
(16) Taton, T. A.; Mirkin, C. A.; Letsinger, R. L. *Science* **2000**, *289*, 1757–1760.
(17) Fritz, J.; Baller, M. K.; Lang, H. P.; Rothuizen, H.; Vettiger, P.; Meyer, E.; Guntherodt, H. J.; Gerber, C.; Gimzewski, J. K. *Science* **2000**, *288*, 316–318.
(18) Samorì, B.; Zuccheri, G. *Angew. Chem., Int. Ed.* **2005**, *44*, 1166–1181.
(19) Yan, H.; Park, S. H.; Finkelstein, G.; Reif, J. H.; LaBean, T. H. *Science* **2003**, *301*, 1882–1884.
(20) Gothelf, K. V.; LaBean, T. H. *Org. Biomol. Chem.* **2005**, *3*, 4023–4037.
(21) Mao, C. D.; LaBean, T. H.; Reif, J. H.; Seeman, N. C. *Nature* **2000**, *407*, 493–496.
(22) Fasel, R.; Parschau, M.; Ernst, K.-H. *Angew. Chem., Int. Ed.* **2003**, *42*, 5178–5181.
(23) Barth, J. V. *Annu. Rev. Phys. Chem.* **2007**, *58*, 375–407.
(24) Grill, L.; Dyer, M.; Lafferentz, L.; Peters, M. V.; Hecht, S. *Nat. Nanotechnol.* **2007**, *2*, 687–691.
(25) Pawin, G.; Wong, K. L.; Kwon, K.-Y.; Bartels, L. *Science* **2006**, *313*, 961–962.
(26) Blunt, M. O.; Russell, J. C.; Gimenez-Lopez, M. D. C.; Garrahan, J. P.; Lin, X.; Schroder, M.; Champness, N. R.; Beton, P. H. *Science* **2008**, *322*, 1077–1081.
(27) Tomba, G.; Ciacchi, L. C.; De Vita, A. *Adv. Mater.* **2009**, *21*, 1055–1066.
(28) Heckl, W. M.; Smith, D. P. E.; Binnig, G.; Klagges, H.; Hänsch, T. W.; Maddocks, J. *Proc. Natl. Acad. Sci. U.S.A.* **1991**, *88*, 8003–8005.
(29) Tao, N. J.; Derose, J. A.; Lindsay, S. M. *J. Phys. Chem.* **1993**, *97*, 910–919.
(30) Tanaka, H.; Nakawaga, T.; Kawai, T. *Surf. Sci.* **1996**, *364*, L575−L579.
(31) Sowerby, S. J.; Edelwirth, M.; Heckl, W. M. *J. Phys. Chem. B* **1998**, *102*, 5914–5922.
(32) Sowerby, S. J.; Stockwell, P. A.; Heckl, W. M.; Petersen, G. B. *Origins Life Evol. Biosphere* **2000**, *30*, 81–99.
(33) Otero, R.; Schöck, M.; Molina, L. M.; Lægsgaard, E.; Stensgaard, I.; Hammer, B.; Besenbacher, F. *Angew. Chem., Int. Ed.* **2005**, *44*, 2270–2275.
(34) Gottarelli, G.; Masiero, S.; Mezzina, E.; Pieraccini, S.; Rabe, J. P.; Samori, P.; Spada, G. P. *Chem.—Eur. J.* **2000**, *6*, 3242–3248.
(35) Kelly, R. E. A.; Kantorovich, L. N. *Surf. Sci.* **2005**, *589*, 139–152.
(36) Perdigão, L. M. A.; Staniec, P. A.; Champness, N. R.; Kelly, R. E. A.; Kantorovich, L. N.; Beton, P. H. *Phys. Rev. B* **2006**, *73*, 195423.
(37) Kelly, R. E. A.; Kantorovich, L. N. *J. Mater. Chem.* **2006**, *16*, 1894–1905.
(38) Mamdouh, W.; Dong, M.; Kelly, R. E. A.; Kantorovich, L. N.; Besenbacher, L. N. *J. Phys. Chem. B* **2007**, *111*, 12048.
(39) Otero, R.; Lukas, M.; Kelly, R. E. A.; Xu, W.; Lægsgaard, E.; Stensgaard, I.; Kantorovich, L. N.; Besenbacher, F. *Science* **2008**, *319*, 312–315.
(40) Kelly, R. E. A.; Lukas, M.; Kantorovich, L. N.; Otero, R.; Xu, W.; Mura, M.; Lægsgaard, E.; Stensgaard, I.; Besenbacher, F. *J. Chem. Phys.* **2008**, *129*, 184707.
(41) Kelly, R. E. A.; Xu, W.; Lukas, M.; Otero, R.; Mura, M.; Lee, Y. J.; Lægsgaard, E.; Stensgaard, I.; Kantorovich, L. N.; Besenbacher, F. *Small* **2008**, *4*, 1494–1500.
(42) Lukas, M.; Kelly, R. E. A.; Kantorovich, L. N.; Otero, R.; Xu, W.; Lægsgaard, E.; Stensgaard, I.; Besenbacher, F. *J. Chem. Phys.* **2009**, *130*, 024705.
(43) Xu, W.; Kelly, R. E. A.; Otero, R.; Schöck, M.; Lægsgaard, E.; Stensgaard, I.; Kantorovich, L. N.; Besenbacher, F. *Small* **2007**, *3*, 2011–2014.
(44) Demers, L. M.; Östblom, M.; Zhang, H.; Jang, N.-H.; Liedberg, B.; Mirkin, C. A. *J. Am. Chem. Soc.* **2002**, *124*, 11248.
(45) Chen, Q.; Richardson, N. V. *Nat. Mater.* **2003**, *2*, 324.
(46) Domke, K. F.; Zhang, D.; Pettinger, B. *J. Am. Chem. Soc.* **2007**, *129*, 6708.
(47) Xu, S.; Dong, M.; Rauls, E.; Otero, R.; Linderoth, T. R.; Besenbacher, F. *Nano Lett.* **2006**, *6*, 1434–1438.
(48) Mamdouh, W.; Dong, M.; Xu, S.; Rauls, E.; Besenbacher, F. *J. Am. Chem. Soc.* **2006**, *128*, 13305–13311.
(49) Otero, R.; Xu, W.; Lukas, M.; Kelly, R. E. A.; Lægsgaard, E.; Stensgaard, I.; Kjems, J.; Kantorovich, L. N.; Besenbacher, F. *Angew. Chem., Int. Ed.* **2008**, 9673–9676.
(50) Mamdouh, W.; Kelly, R. E. A.; Dong, M.; Kantorovich, L. N.; Besenbacher, F. *J. Am. Chem. Soc.* **2008**, *130*, 695–702.
(51) Kumar, A. M. S.; Fox, J. D.; Buerkle, L. E.; Marchant, R. E.; Rowan, S. J. *Langmuir* **2009**, *25*, 653–656.
(52) Davies, J. T. *Angew. Chem., Int. Ed.* **2004**, *43*, 668.
(53) Lavergne, O.; Fernandes, A.-C.; Bréhu, L.; Sidhu, A.; Brézak, M.-C.; Prévost, G.; Ducommun, B.; Contour-Galcera, M.-O. *Bioorg. Med. Chem. Lett.* **2006**, *16*, 171–175.
(54) http://www.imagemet.com.
(55) Samorí, P.; Engelkamp, H.; de Witte, P.; Rowan, A. E.; Note, R. J. M.; Rabe, J. P. *Angew. Chem.* **2001**, *113*, 2410−2412; *Angew. Chem., Int. Ed.* **2001**, *40*, 2348−2350.
(56) Ordejon, P.; Artacho, E.; Soler, J. M. *Phys. Rev. B* **1996**, *53*, R10441−R10444.
(57) Soler, J. M.; Artacho, E.; Gale, J. D.; Garcia, A.; Junquera, J.; Ordejon, P.; Sanchez-Portal, D. *J. Phys.: Condens. Matter* **2002**, *14*, 2745–2779.
(58) Kelly, R. E. A.; Lee, Y. J.; Kantorovich, L. N. *J. Phys. Chem. B* **2005**, *109*, 22045–22052.
(59) Kelly, R. E. A.; Kantorovich, L. N. *J. Phys. Chem. B* **2006**, *110*, 2249–2255.
(60) Kelly, R. E. A.; Lee, Y. J.; Kantorovich, L. N. *J. Phys. Chem. B* **2005**, *109*, 11933–11939.
(61) Kelly, R. E. A.; Kantorovich, L. N. *J. Phys. Chem. C* **2007**, *111*, 3883–3892.
(62) Sponer, J.; Jurecka, P.; Hobza, P. *J. Am. Chem. Soc.* **2004**, *126*, 10142.
(63) Kelly, R. E. A.; Kantorovich, L. N. To be submitted for publication.

JP9029419